Abyssal Mixing: Where It Is Not

ERIC KUNZE

School of Oceanography, University of Washington, Seattle, Washington

THOMAS B. SANFORD

Applied Physics Laboratory, University of Washington, Seattle, Washington

5 June 1995 and 23 January 1996

ABSTRACT

A parameterization based on internal wave/wave interaction theory, which infers turbulence production from finescale internal wave shear, is applied to 114 full-water-depth velocity profiles in the Sargasso Sea. An average eddy diffusivity of 0.1×10^{-4} m^2 s^{-1}, independent of depth, is inferred. This value is consistent with full-water-depth microstructure measurements from abyssal basins in the eastern North Atlantic and eastern North Pacific. It is an order of magnitude smaller than the values inferred from a simple vertical advection–diffusion balance or bulk budgets. Thus, the mixing needed to close deep global water-mass budgets does not appear to occur over midlatitude abyssal plains. This suggests that ocean mixing is either (i) confined to boundary layers as in ideal thermocline theory or (ii) localized to hotspots, such as over rough topography or restrictive passages. Abyssal diffusivities do not display any dependence on bottom slope for slopes less than 7×10^{-2} based on 5–10 km bathymetry, but are higher over convex than concave topography and higher in stronger bottom currents.

1. Introduction

A dominant paradigm for the role of ocean mixing on the large-scale circulation has been the vertical advection–diffusion balance for the main pycnocline

$$w\rho_z = (K_\rho \rho_z)_z \approx K_\rho \rho_{zz} \Rightarrow \frac{K_\rho}{w} \approx \frac{\rho_z}{\rho_{zz}} = 1300 \text{ m}, \quad (1)$$

(Munk 1966). Assuming uniform vertical velocities $w = 0.5–1$ cm day^{-1} inferred from deep-water formation rates (e.g., Gill 1973; Carmack and Foster 1975), (1) implies diapycnal eddy diffusivities of $\sim 10^{-4}$ m^2 s^{-1}. However, two decades of microstructure measurements (Moum and Osborn 1986; Gregg 1987; Toole et al. 1994) and a deliberate tracer-release experiment (Ledwell et al. 1993) find diffusivities in the upper 1000 m of only $(0.05–0.15) \times 10^{-4}$ m^2 s^{-1}, well below the abyssal-recipes value. It would appear that the vertical advection–diffusion balance does not hold in the upper ocean; lateral processes must be important (Jenkins 1980; McWilliams 1983). This is the underlying assumption behind ideal thermocline theory (Welander 1959; Luyten et al. 1983; Hautala and Riser 1989), which confines diapycnal mixing to the surface or bottom boundary.

The vertical advection–diffusion balance was originally intended to model abyssal not upper-ocean waters. It continues to be used with the resurgence of interest in Stommel and Arons (1960) abyssal circulation (e.g., Kawase 1987; Speer and McCartney 1992). However, as in the pycnocline, deep stratification could be controlled by boundary mixing and isopycnal stirring (Munk 1966; Armi 1978). The presence of radon 222 maxima as much as 1 km above the bottom in over half the GEOSECS profiles (Sarmiento et al. 1976) suggests that lateral advective processes may play a large role.

Bulk budget estimates of mixing in abyssal basins range from 4×10^{-4} m^2 s^{-1} (Hogg et al. 1982; Saunders 1987) to as low as 0.1×10^{-4} m^2 s^{-1} (Whitehead 1989). Whitehead demonstrates that bulk estimates can be very sensitive to poorly known basin topography and assumptions about the dynamics and structure of the inflows. More importantly, bulk estimates do not distinguish between boundary and interior mixing.

Full-water-depth microstructure measurements (Toole et al. 1994) find eddy diffusivities of $(0.2–0.3) \times 10^{-4}$ m^2 s^{-1} over abyssal plains. However, they report values as high as 3×10^{-4} m^2 s^{-1} within a few kilometers of a seamount's flanks. This suggests that sloping topography or bottom roughness might provide sites of elevated abyssal mixing. High diffusivities are reported atop seamounts ($\sim 10 \times 10^{-4}$ m^2 s^{-1}, Nabatov and Ozmidov 1988; Toole et al. 1996; Lueck and Mudge 1995, manuscript submitted to *Science*) and have been inferred in the vicinity of

Corresponding author address: Dr. Eric Kunze, School of Oceanography, University of Washington, Box 357940, Seattle, WA 98195.
E-mail: kunze@ocean.washington.edu

rough topography (Armi 1978; Johnson and Sanford 1980; Gargett 1984; Lueck et al. 1983; Kunze et al. 1992; Ffield and Gordon 1992). Recent microstructure measurements in the Romanche Fracture Zone have found eddy diffusivities in the abyssal 500 m over sills of 100×10^{-4} m^2 s^{-1} and over rough topography of 10×10^{-4} m^2 s^{-1} (Polzin et al. 1996b).

Gregg (1989) and Polzin et al. (1995) argue that elevated mixing requires internal wave shear or strain above GM levels on the basis of their verification of a turbulence-production parameterization originally put forward by Henyey et al. (1986). This scaling links the turbulent dissipation rate ϵ to finescale shear $V_z = \sqrt{u_z^2 + v_z^2}$ and strain ξ_z levels, which control the rate at which wave–wave interactions transfer energy toward high vertical wavenumber. Elevated internal wave levels have been reported near the bottom, particularly over rough topography (Wunsch and Webb 1979; Fu 1981; Eriksen 1982; Kunze and Sanford 1986; Padman and Dillon 1991; Kunze et al. 1992; Wijesekera et al. 1993; Eriksen 1996).

Here, we will apply the Gregg–Henyey–Polzin parameterization to full-water-depth velocity profiles from the Sargasso Sea. After describing the parameterization and the data, we show that this methodology predicts eddy diffusivities of $\sim 0.1 \times 10^{-4}$ m^2 s^{-1} independent of depth, as previously found by Toole et al. (1994) with full-water-depth microstructure measurements over similarly smooth abyssal plains in the eastern North Atlantic and eastern North Pacific. We conclude that, if strong mixing is to be found in the stratified deep ocean, it is confined to sites of rough bathymetry.

2. The Gregg–Henyey–Polzin parameterization

Internal wave–wave interactions, based on either weak resonant (McComas and Müller 1981) or ray tracing (Henyey et al. 1986; Sun et al. 1996) techniques, flux energy through the Garrett and Munk (GM76; Garrett and Munk 1975; Cairns and Williams 1976) model spectrum to high vertical wavenumber and turbulent production at a rate that scales with buoyancy frequency N and spectral energy level E_0 as

$$\epsilon \propto N^2 E_0^2. \tag{2}$$

Gregg (1989) showed that normalizing the observed turbulent dissipation rate ϵ by

$$\epsilon = \epsilon_0 \frac{N^2}{N_0^2} \frac{V_z^4}{{}_{\rm GM}V_z^4} = \epsilon_0 \frac{N^2}{N_0^2} \frac{\langle V_z^2 \rangle^2}{\langle {}_{\rm GM}V_z^2 \rangle^2}, \tag{3}$$

reduced scatter to within a factor of 2 in a variety of open-ocean internal wave fields, where the spectral level is expressed in terms of the finescale shear variance $\langle V_z^2 \rangle$ rather than the spectral energy level E_0, the normalizing buoyancy frequency $N_0 = 5.2 \times 10^{-3}$ s^{-1}, $\epsilon_0 = 7.8 \times 10^{-10}$ W kg^{-1} and $\langle {}_{\rm GM}V_z^2 \rangle$ is the equivalent GM76 shear variance.

Wijesekera et al. (1993) found that (3) greatly underestimated dissipation rates over Yermak Plateau where the internal wave field contained far more high-frequency wave energy than the GM76 model. This discrepancy appears to have been resolved (see next paragraph). Scaling (3) also fails on the equator (Peters et al. 1995) where the internal wave field is not GM-like due to vanishing Coriolis frequency and strong mean vertical shears.

Following up Henyey's (1991) suggested modification for non-GM spectral shapes, Polzin et al. (1995) found that normalizing observed dissipation rates by the scaling

$$\epsilon = \epsilon_0 \frac{N^2}{N_0^2} \frac{\langle V_z^2 \rangle^2}{\langle {}_{\rm GM}V_z^2 \rangle^2} f(R_\omega) \tag{4}$$

collapsed scatter to within a factor of 2 for non-GM frequency spectra, where the ratio of shear to strain $R_\omega = \langle V_z^2 \rangle / (N^2 \langle \xi_z^2 \rangle)$ [$=3.0$ for GM76] is a proxy measure for the rms internal-wave aspect ratio $\langle k_H / k_z \rangle$, and

$$f(R_\omega) = \left[\frac{{}_{\rm GM}R_\omega}{R_\omega} \right] \left[\frac{R_\omega + 1}{{}_{\rm GM}R_\omega + 1} \right] \sqrt{\frac{{}_{\rm GM}R_\omega - 1}{R_\omega - 1}}. \tag{5}$$

This modification accounts for most of the large discrepancy from Gregg's formula (3) found over the Yermak Plateau by Wijesekera et al. (1993). Polzin et al. (1995) found that horizontal anisotropy, vertical asymmetry, and the vertical wavenumber spectral shape did not produce any systematic deviation from (4), although this may have been based on insufficient data.

From Osborn (1980), the diapycnal eddy diffusivity

$$K_\rho = \frac{e\epsilon}{N^2} = K_0 \frac{\langle V_z^2 \rangle^2}{\langle {}_{\rm GM}V_z^2 \rangle^2} f(R_\omega), \tag{6}$$

where the mixing efficiency $e \leq 0.2$ (Osborn 1980; Thompson 1980; McEwan 1980; Itsweire et al. 1986; Oakey 1982; Peters et al. 1988; Moum et al. 1989) and the eddy diffusivity $K_0 \leq 0.05 \times 10^{-4}$ m^2 s^{-1} corresponds to a GM-level spectrum. For GM spectral levels [$\langle V_z^2 \rangle = \langle {}_{\rm GM}V_z^2 \rangle$ and $f(R_\omega) = 1.0$], the eddy diffusivity is an order of magnitude smaller than predicted from the vertical advection–diffusion balance (Munk 1966). Gregg (1989) and Polzin et al. (1995) argued that higher diffusivities require internal wave shears V_z or strains ξ_z elevated above GM levels.

3. Measurements

In the following, we apply (3) and (6) to 114 full-water-depth velocity profiles from the Sargasso Sea in the western North Atlantic. The profiles have 10-m vertical resolution and 1 cm s^{-1} rms errors. They include 58 profiles collected in May–June 1973 during MODE (the MODE Group 1978) with The ElectroMagnetic Velocity Profiler (EMVP) and 56 profiles collected in

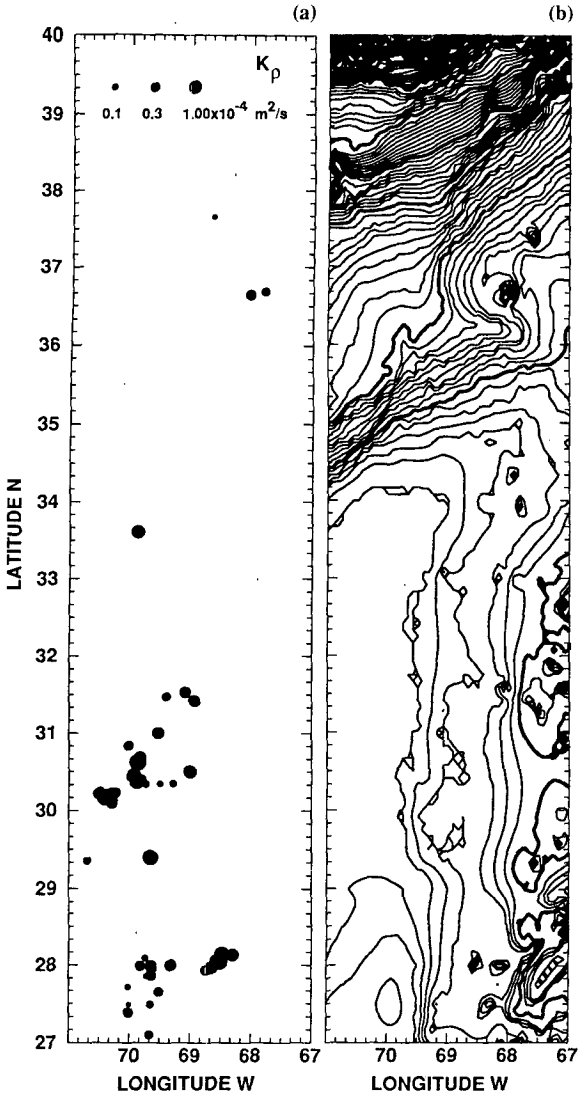

FIG. 1. Charts of full-water-depth velocity profile positions (a) and bathymetry (b) in the western North Atlantic. The bathymetric contour interval is 50 m. MODE '73 drops lie south of 28°N and POLYMODE '78 drops north. The northernmost two stations are on the continental slope and Gulf Stream, respectively. MODE profiles east of 69°W were over rough topography. Stations near 36°40′N were over the summit and lower flanks of Caryn Seamount. The areas of the dots are proportional to estimates of $\log(K_\rho)$ at 4500–5500-m depth.

June 1978 during POLYMODE (McWilliams et al. 1983) with the Absolute Velocity Profiler (AVP). The sampling and bathymetry are shown in Fig. 1a. MODE drops lie south of 28°N while POLYMODE drops lie north of 28°N. POLYMODE profiles near 30°10′N, 70°30′W were in a subthermocline lens of anomalous water (Elliott and Sanford 1986a,b). Those near 36°40′N, 68°W were on the summit and flanks of Caryn Seamount (Kunze and Sanford 1986). We note that barotropic tidal currents are less than 0.5 cm s^{-1} in the Sargasso Sea (Schwiderski 1979; Luyten and Stommel 1991). Measured AVP currents in the bottom 1000 m show a mean southwestward jet of 10–14 cm s^{-1} between 30°N and 32°N.

EMVP (Sanford et al. 1978) and AVP (Sanford et al. 1985) are freefall profilers. Both determine the zonal and meridional velocities electromagnetically by measuring the voltage drop across the instrument's insulating body induced by the seawater's movement in the earth's magnetic field. This provides the velocity relative to a depth-independent constant. The AVP makes these velocities absolute with acoustic Doppler echoes off the seafloor. Velocities were sampled redundantly with two independent pairs of electrodes. Data were collected during both descent and ascent to within 10 m of the bottom.

The MODE EMVP and POLYMODE AVP profiles include temperature but not salinity. The average buoyancy frequency profile from MODE CTD measure-

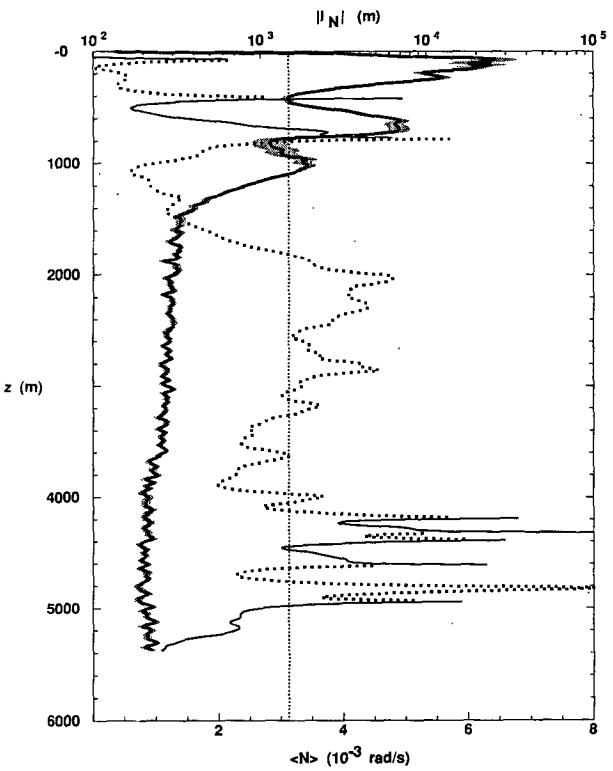

FIG. 2. The average buoyancy frequency profile $\bar{N}(z)$ (thick solid curve) and buoyancy lengthscale $l_N = \bar{N}^2/\bar{N}_z^2 = \rho_{\bar{z}}/\rho_{zz}$ (thick dotted, thin solid) for the MODE region. Stippling about $\bar{N}$ denotes one standard error. Solid l_N denotes negative curvature in the density profile, ρ_{zz}, while dotted indicates positive curvature. The buoyancy frequency profile exhibits three maxima and two minima in the upper 1200 m and is approximately uniform at 10^{-3} rad s^{-1} below 1500-m depth. For a vertical advection–diffusion balance, the buoyancy lengthscale l_N is equal to K_ρ/w. It is roughly equal to its canonical GM 1300 m (dotted vertical line) between 2000-m and 4000-m depth. Wild fluctuations below 4000 m are due to near-zero values of N_z^2.

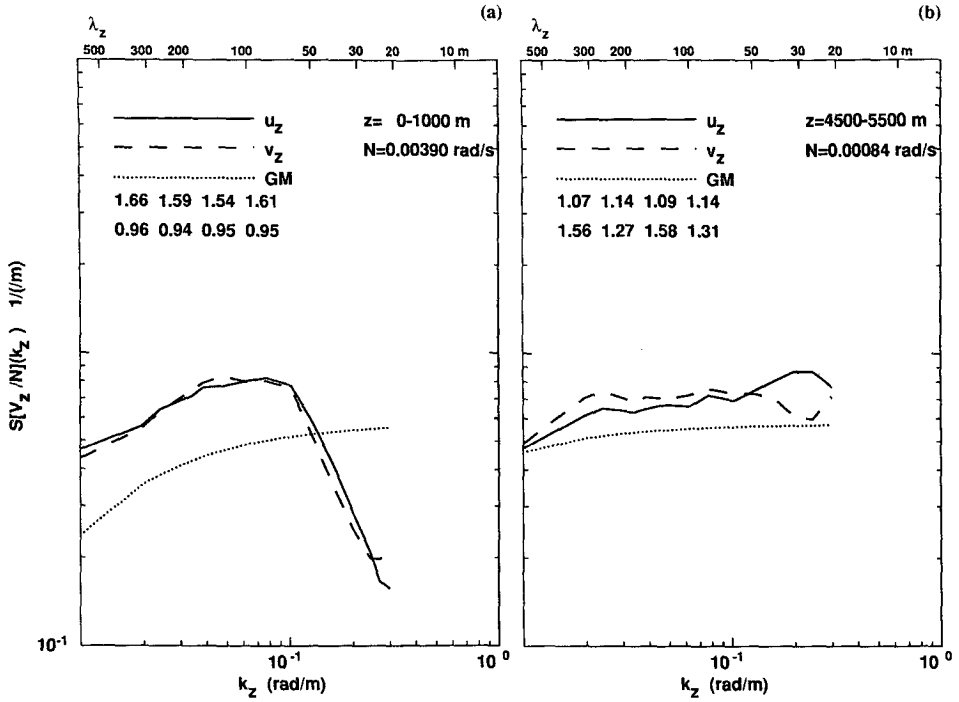

FIG. 3. Avcrage vertical wavenumber spectra for Froude number V_z/N in the upper 1000 m (a) and abyssal 4500–5500 m (b) of the Sargasso Sea. The solid and dashed lines are the observed east u_z/N and north v_z/N component Froude number spectra. The dotted curve corresponds to the GM76 component (e.g., u_z/N) spectra. Numbers in the upper-left quadrant are the GM-normalized variances of east and north velocities, u_1, v_1, u_2, and v_2 (upper line), and east and north shears, u_{z_1}, v_{z_1}, u_{z_2}, and v_{z_2}, (lower line) from the two independent electrode pairs. The shallow spectra (a) fall off as $k_z^{-3/2}$ for wavelengths $\lambda_z < 50$ m, while the abyssal (b) and GM76 model spectra do not display a change in slope until $\lambda_z < 10$ m.

ments is shown in Fig. 2. This average profile will be used for all the MODE and POLYMODE profiles. The buoyancy lengthscale $l_N = N^2/N_z^2$ (thick dotted curve in Fig. 2) exhibits wide variability. Between 2000-m and 4000-m depth, it has the canonical value of ~1300 m used in the GM76 model spectrum (7). Below 4000 m, it exhibits wild fluctuations because N_z^2 is small.

In neither dataset is the temperature noise level small enough to resolve the finescale strain $\xi_z = (\bar{T}_z - T_z)/\bar{T}_z = (\bar{N}^2 - N^2)/\bar{N}^2$ with any confidence in abyssal waters. Therefore, finescale analysis will be limited to shear, and a GM76 frequency spectra will be assumed [$f(R_\omega) = 1.0$]. A greater contribution from near-inertial waves than in the GM76 model would produce weaker turbulent mixing, a greater contribution from higher-frequency waves stronger mixing.

4. Results

a. *Vertical wavenumber spectra*

Finescale shear variance levels $\langle V_z^2 \rangle$ are determined by integrating the observed spectra in nonoverlapping 640-m depth intervals from the lowest resolved vertical wavenumber ($\lambda_z = 640$ m) to the highest resolved wavenumber ($\lambda_z = 20$ m), or while the Froude number variance $\langle V_z^2 \rangle / N^2 = \int_0^{k_{z_1}} S[V_z/N](k_z)dk_z$ is less than 0.7, whichever comes first. Except for a few abyssal depth bins, it was usually the former. This follows the methodology of Polzin et al. (1995) in response to Gargett's (1990) criticisms of Gregg (1989) using 10-m first-differences to estimate the shear regardless of possible distortions to the vertical wavenumber spectral shape. The GM shear variance is obtained by treating the GM76 model spectrum for Froude number

$$S_{GM}[V_z/N](k_z)dk_z = \frac{3\pi E_0 l_N j^*}{2} \frac{k_z^2 dk_z}{(k_z + k_{z^*})^2} \quad (7)$$

(Gregg and Kunze 1991) in the same way as the data where the nondimensional GM spectral level $E_0 = 6.3 \times 10^{-5}$, the buoyancy frequency profile lengthscale $l_N = 1300$ m, the vertical wavenumber $k_z = \pi N j/(l_N N_0)$, and the peak mode number $j^* = 3$. Spectrum (7) is flat for vertical wavenumbers $k_z \gg k_{z^*}(\lambda_{z^*} = 867$ m).

Average vertical wavenumber spectra for Froude number from depths 0–1000 m and 4500–5500 m are compared with the GM76 model in Fig. 3. In the upper 1000 m (Fig. 3a), spectral levels are 1.6 times higher than GM for vertical wavelengths $\lambda_z > 70$ m. At higher

wavenumbers, these spectra exhibit a change in slope from ~0 (flat) to −1.5 at a vertical wavelength $\lambda_z = 50$ m, and drop below the GM76 spectrum. This change in slope occurs at much larger wavelengths than the 10-m wavelength usually reported (Gargett et al. 1981; Duda and Cox 1989; Gregg et al. 1993). It is consistent neither with (i) saturated spectra arguments based on the low-wavenumber level of the spectra, $Ek_{z_c} = \text{const}$ (Munk 1981) nor (ii) the rolloff occurring at $\langle V_z^2\rangle/N^2 = 0.5 - 0.8$ reported by Gregg et al. (1993) since, shallower than 3000-m depth, the observed rolloff occurs at $\langle V_z^2\rangle/N^2 = 0.2$. Sanford (1991) hypothesized that it might be the result of critical layers in the mean first-mode shear of ~20 cm s^{-1} in the upper 1500 m (his Fig. 3). However, Polzin et al. (1996a) show that mean shear will enhance the spectral energy flux to high wavenumber and turbulence production only if the mean Froude number $\langle V_z\rangle/N$ exceeds 0.2, and it is less than 0.15 here. Moreover, the change in spectral slope occurs at the same wavenumber in the anticyclonic lens where shear is larger than in the rest of the profiles.

In the context of this paper, the low-wavenumber change in spectral slope raises an ambiguity about whether the shear spectra should be integrated to the break in slope, which would lead to higher shear variance ratios $\langle V_z^2\rangle/\langle_{GM}V_z^2\rangle$, or while the shear variance $\langle V_z^2\rangle \leq 0.7N^2$. The latter are displayed here following Polzin et al. (1995). This may underestimate the normalized shear variance $\langle V_z^2\rangle/\langle_{GM}V_z^2\rangle$ by a factor of 0.6, and the turbulent dissipation rate ϵ and eddy diffusivity K_ρ by a factor of 0.4 in the upper 3000 m, where the break in slope at $\lambda_z = 70$ m is found. This does not affect the main conclusions, in particular, the abyssal values which are the focus of this paper.

In the abyssal 4500–5500 m of the ocean (Fig. 3b), the observed spectra are flat and lie above the GM76 model at all but the lowest wavenumbers. Integrated to 20-m vertical wavelength, the GM-normalized shear variance $\langle V_z^2\rangle/\langle_{GM}V_z^2\rangle$ is 1.5 on average where the 20-m $\langle_{GM}V_z^2\rangle = 0.35N^2$.

b. Shear variances

Figure 4 displays profiles of GM-normalized shear variance

$$\frac{\langle V_z^2\rangle}{\langle_{GM}V_z^2\rangle} = \frac{\int_0^{k_{z_1}} S[V_z/N](k_z)\cdot dk_z}{\int_0^{k_{z_1}} S_{GM}[V_z/N](k_z)\cdot dk_z}.$$

As no significant difference was found between the up- and down-profiles or the MODE and POLYMODE numbers, they have been merged together. Spectral levels were extracted from nonoverlapping 640-m thick depth bins starting at the bottom. This accounts for clumping of the data points with depth. The absence of depth dependence in the raw data is substantiated in the averages (striped curves), which show that the finescale shear is at most marginally elevated above GM76 values in the abyssal 1500 m of the Sargasso Sea. Augmenting values in the upper 2000 m by a factor of 1.6 to correct for possible underestimation due to integrating beyond the break in slope would not substantially alter the mean profile.

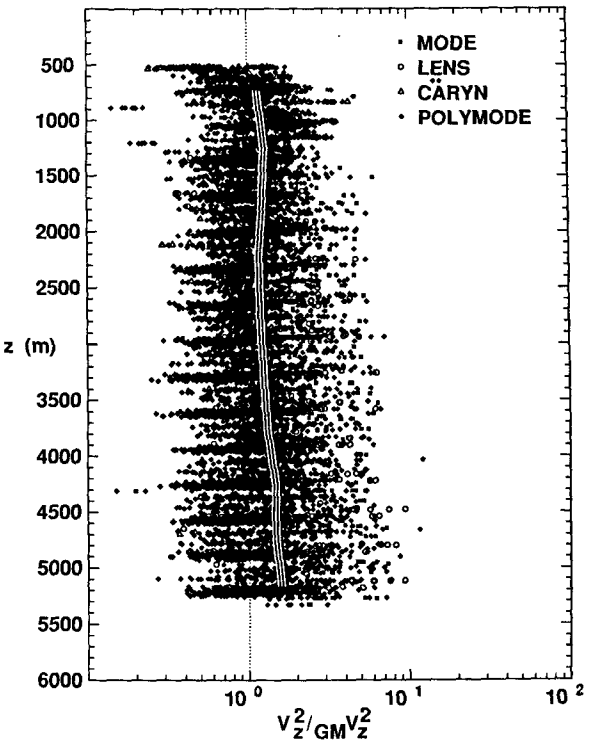

FIG. 4. Profiles of spectral shear variance $\langle V_z^2\rangle = \int_0^{k_{z_1}} S[V_z](k_z)dk_z$ normalized by the equivalent GM shear variance $\langle_{GM}V_z^2\rangle$ for all MODE and POLYMODE profiles. Individual estimates from both up- and down-profiles and from the two independent velocity sensors are displayed. Mid-thermocline lens (open circles) and Caryn Seamount (open triangles) profiles are subsets of the POLYMODE data. The depth-smoothed ratios (striped curve) lie between 1.0 and 2.0, almost independent of depth.

c. Parameterized turbulence

Inserting values of $\langle V_z^2\rangle/\langle_{GM}V_z^2\rangle$ from Fig. 4 into the Gregg–Henyey parameterizations (4) and (6) with the Polzin et al. (1995) correction for non-GM frequency spectral shapes $f(R_\omega)$ set equal to one, profiles of inferred turbulent dissipation rate ϵ and eddy diffusivity K_ρ are displayed in Fig. 5. The inferred average turbulent dissipation rate (Fig. 5a) decreases from $\sim 10^{-9}$ W kg^{-1} at 700-m depth to $\sim 10^{-10}$ W kg^{-1} at 1700-m depth and is roughly independent of depth below 2000 m, following the depth dependence of the stratification $\bar{N}^2$ (Fig. 2). As a result, the inferred average eddy diffusivity

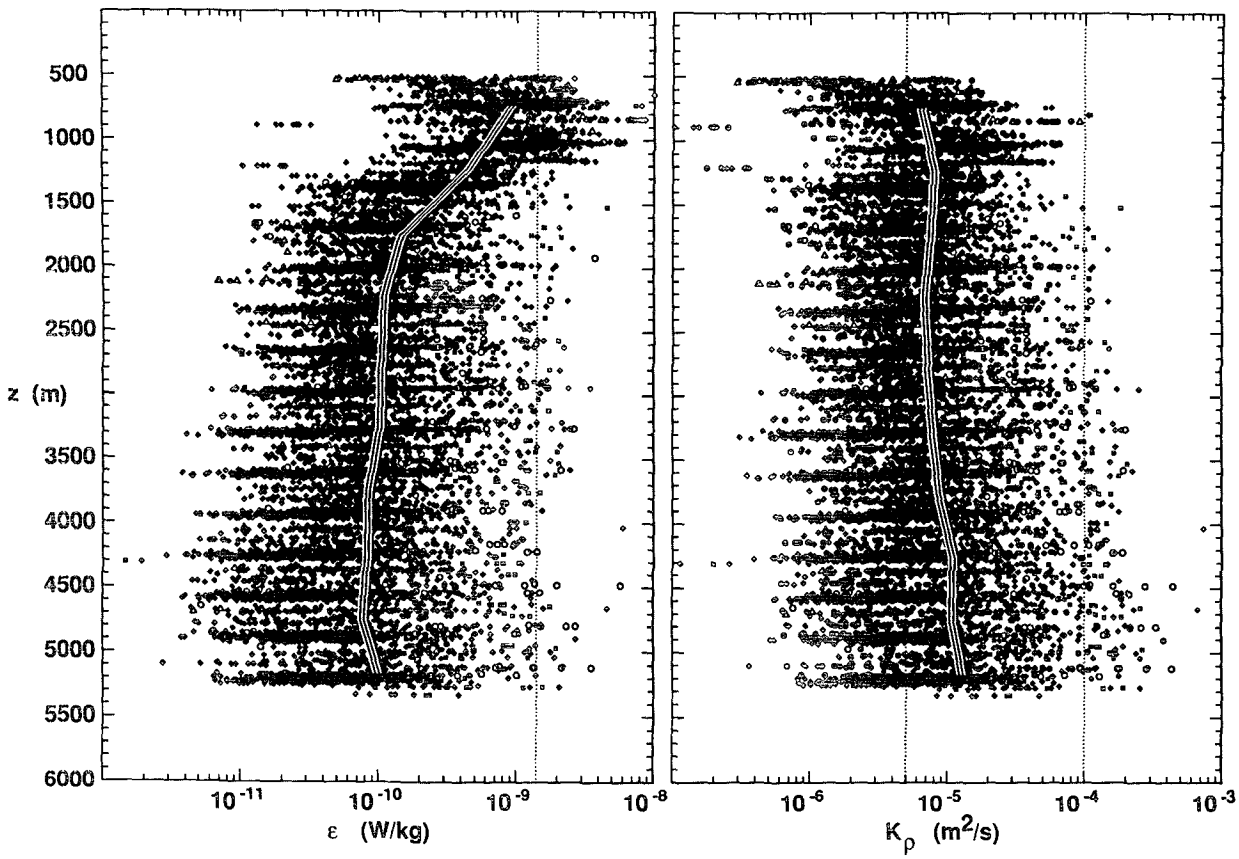

FIG. 5. Profiles of turbulent dissipation rate ϵ inferred from the Gregg–Henyey–Polzin parameterization (4) with $f(R_\omega)$ set equal to one (left panel) and eddy diffusivity K_ρ (6) (right panel) for all MODE and POLYMODE profiles. Individual estimates are shown as symbols (see Fig. 4 caption). Below 1500-m depth, the depth-smoothed dissipation rate (striped curve) is nearly constant at $\epsilon \sim 10^{-10}$ W kg^{-1}. The depth-smoothed eddy diffusivity K_ρ is nearly independent of depth throughout, increasing only slightly from 0.07×10^{-4} to 0.15×10^{-4} m^2 s^{-1} in the bottom 1000 m.

$K_\rho \leq 0.2\epsilon/\bar{N}^2$ (Fig. 5b) is nearly uniform with depth at $\sim 0.1 \times 10^{-4}$ m^2 s^{-1}. Augmenting ϵ and K_ρ by a factor of 2.5 in the upper 3000 m—to account for our choosing to integrate the observed and GM76 spectra while the observed $\langle V_z^2 \rangle / N^2$ is less than 0.7 rather than to the break in slope—does not substantially alter the depth independence of the eddy diffusivity. The raw K_ρ display a roughly log normal distribution (Fig. 6).

d. Dependence on bottom slopes and currents

While higher abyssal diffusivities appear to be associated with rough topography around 28°N, 68°30′W (Fig. 1), equally high diffusivities are found near 30°30′N, 70°W where the bathymetry is smooth. To better quantify the relationship between inferred eddy diffusivity and topography, abyssal eddy diffusivities are plotted against local (within 10 km) rms bottom slopes in Fig. 7a. The rms bottom slopes are computed from NGDC ETOPO5 dataset with a horizontal resolution of 5′ (5–9 km) in latitude and longitude. No obvious dependence is evident over the 10^{-5} to 10^{-1} range in slope (Fig. 7a); abyssal diffusivities are $(0.1–0.2) \times 10^{-4}$ m^2 s^{-1} as found in the overlying water. This lack of enhancement is inconsistent with Garrett and Gilbert's (1988) predictions for the energy flux available for mixing based on a GM76 internal wave field reflecting off a sloping bottom; the dotted curve in Fig. 7a assumes that Garrett and Gilbert's predicted energy flux is lost to turbulence in a layer 640 m thick, the thickness of our spectral bins and the thickness of stratified turbulent benthic boundary layers observed by microstructure profilers (Toole et al. 1994; Polzin et al. 1996b). [The Garrett and Gilbert predictions do not include any mixing that might be induced by scattering of the barotropic semidiurnal tide. But barotropic tidal currents are less than 0.5 cm s^{-1} in the Sargasso Sea (Schwiderski 1979; Luyten and Stommel 1991). Sjöberg and Stigebrand (1992) and Morozov (1995) predict transfers of energy from the barotropic to the baroclinic tide of less than 10^{-4} W m^{-2} in the Sargasso Sea which, if lost to turbu-

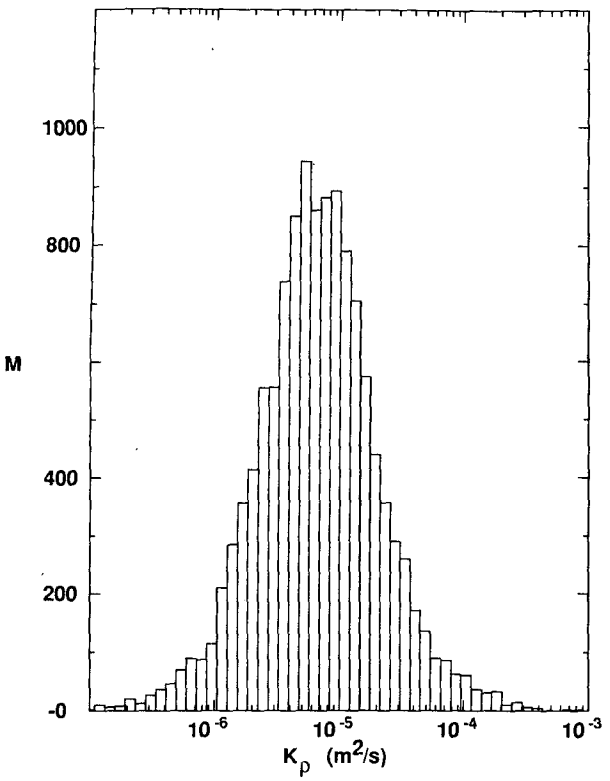

FIG. 6. The probability distribution of inferred eddy diffusivity (6) in all the MODE and POLYMODE profiles (from Fig. 5). The distribution is roughly lognormal.

lence in the bottom 640 m, would produce turbulent dissipation rates of less than 10^{-10} W kg^{-1}.]

The lack of observed enhancement at stronger slopes (Fig. 7a) may be due to destructive interference between reflected waves over concave topography (Gilbert and Garrett 1989)—although Eriksen (1995) finds no evidence for this on the flanks of Fieberling Seamount and argues that critically reflected waves will lose their energy to shear instability before they can destructively interfere. Comparison of profiles over positive and negative topographic curvature reveals that convex topography is more extreme ($\leq 3 \times 10^{-5}$ m^{-1} associated with Caryn Seamount) than concave ($\leq 3 \times 10^{-6}$ m^{-1}). Average eddy diffusivities are $(0.11 \pm 0.01) \times 10^{-4}$ m^2 s^{-1} over concave topography and $(0.29 \pm 0.04) \times 10^{-4}$ m^2 s^{-1} over convex topography with no consistent dependence on the magnitude of the curvature.

The lack of observed enhancement over strongly sloping topography may also be due to inadequate statistics or the coarseness of the ETOPO5 bathymetry. The NGDC ETOPO5 5′ (5–9 km) bathymetry may not resolve all significant slopes. Also, the influence of bathymetry can be nonlocal due to the gentle propagation angles $\Delta z/\Delta r = Cg_z/Cg_H = \tan\alpha$ of reflected waves (e.g., a propagation slope of 10^{-2} corresponds to spreading over 50 km at 500 m above the bottom). We have also neglected the internal wave strain. The steepest slope of 7×10^{-2} reported here corresponds to a critical frequency of $1.5f$, which is too low to produce high strains. However, this again may reflect the coarseness of the bathymetry grid.

Evidence of some topographic effect can be seen in the ratio of clockwise- to counterclockwise-with-depth energy, which shows equipartition of up- and down-

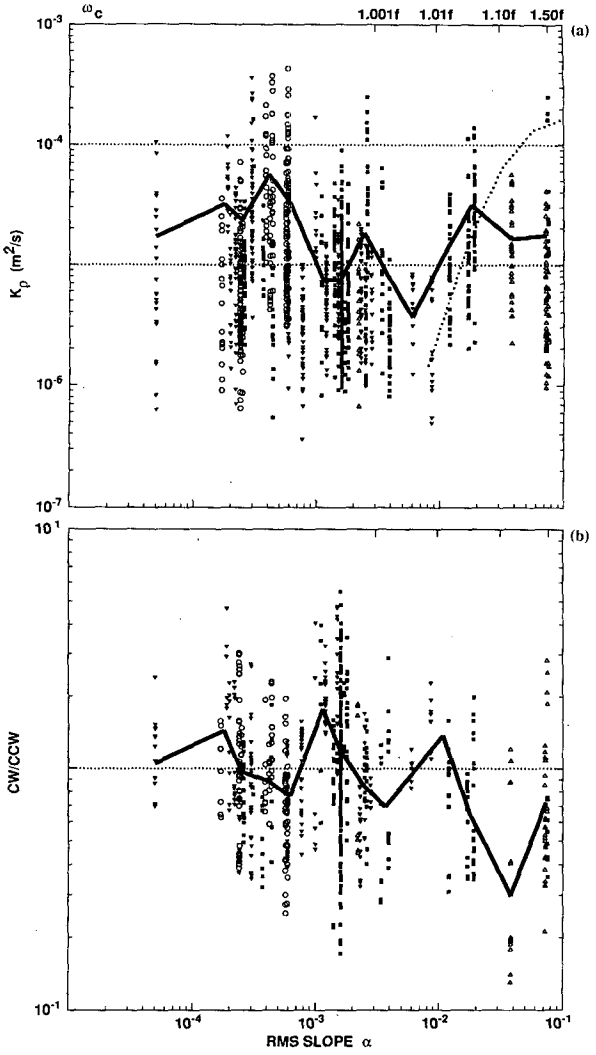

FIG. 7. Inferred eddy diffusivity K_ρ from (6) (a) and the ratio of clockwise- to counterclockwise-with-depth energies CW/CCW (b) in the abyssal 640 m of the ocean binned with respect to 5–9 km rms bottom slope α. The ETOPO5-derived topographic slopes range from 5×10^{-5} to 7×10^{-2} (internal-wave critical reflection frequencies, $\omega_c \leq 1.5f$). Eddy diffusivities (a) of $(1-2) \times 10^{-5}$ m^2 s^{-1} are typical with slightly higher values in the lens profiles (open circles). Inferred eddy diffusivities do not rise above 10^{-4} m^2 s^{-1} for higher bottom slopes, as predicted by the internal wave reflection theory (dotted curve) of Garrett and Gilbert (1988). The rotary energy ratio (b) is near one except for bottom slopes $\alpha > 10^{-2}$ where counterclockwise-with-depth (upward energy propagation) is 2–3 times larger.

going near-inertial energy for bottom slopes weaker than 10^{-2} but a factor of 2–3 dominance of upgoing energy for stronger slopes (Fig. 7b). This was previously noted in the MODE profiles by Leaman (1976). This signal is not seen in the ratio of clockwise- to counterclockwise-with-depth shears, so is confined to vertical wavelengths larger than 100 m. Though not statistically significant, both the energy CW/CCW and shear variance CW_z/CCW_z ratios suggest excess upgoing near-inertial variance for convex curvatures greater than 7×10^{-6} m^{-1} (Fig. 8).

The inferred abyssal diffusivities also display a dependence on near-bottom flow speeds in the POLYMODE absolute velocity profiles, increasing from 0.05 $\times 10^{-4}$ m^2 s^{-1} for speeds less than 2 cm s^{-1} to 0.5 $\times 10^{-4}$ m^2 s^{-1} for speeds exceeding 10 cm s^{-1} (Fig. 9). According to Bell's (1975) topographic generation theory, these mean currents would generate internal waves if they flowed over topography with scales less than 10 km, below the resolution of the ETOPO5 dataset. The data presented here are insufficient to distinguish between the processes of internal wave reflection, scattering, and generation associated with the interactions of internal waves and mean flow with topography but suggest that all of these processes play some role.

5. Conclusions and discussion

a. Conclusions

The Gregg–Henyey–Polzin scaling for turbulent dissipation rate ϵ in terms of finescale internal wave shear V_z and strain ξ_z has previously been found to collapse two-order-of-magnitude scatter in ϵ to within a factor of 2 for GM (Gregg 1989) and non-GM frequency spectral shapes (Polzin et al. 1995). Application of this scaling to 144 full-water-depth velocity profiles from the Sargasso Sea yields a depth-independent diapycnal eddy diffusivity $K_\rho \approx 0.1 \times 10^{-4}$ m^2 s^{-1}, consistent with previous deep microstructure measurements over abyssal plains in the eastern North Atlantic and eastern North Pacific (Toole et al. 1994).

b. Discussion

We conclude that the vertical mixing required to balance the abyssal water-mass budget is absent over midlatitude abyssal plains and a simple vertical advection-diffusion balance cannot be invoked there. The inferred eddy diffusivity is an order of magnitude smaller than values required bulk budgets and for a vertical advection–diffusion balance (1) assuming uniform vertical upwelling over the world's ocean basins (Munk 1966). The weak observed diffusivities leave open two possibilities.

First, mixing may be confined to boundaries (Munk 1966). This is the underlying assumption of ideal thermocline theory (Luyten et al. 1983; Huang 1989; Hautala and Riser 1989) where water properties are conserved in the stratified interior away from boundaries. Moreover, it is consistent with the conclusions of Jenkins (1980) in the main pycnocline and McWilliams (1983) at all depths that horizontal processes play a prominent role in the density conservation equation in the Sargasso Sea.

Second, high abyssal turbulent mixing may be even more localized at hotspots either (i) overlying rough topography or (ii) in restrictive passages and sills. Rough topography would scatter barotropic tides and internal waves to high wavenumber (Eriksen 1982;

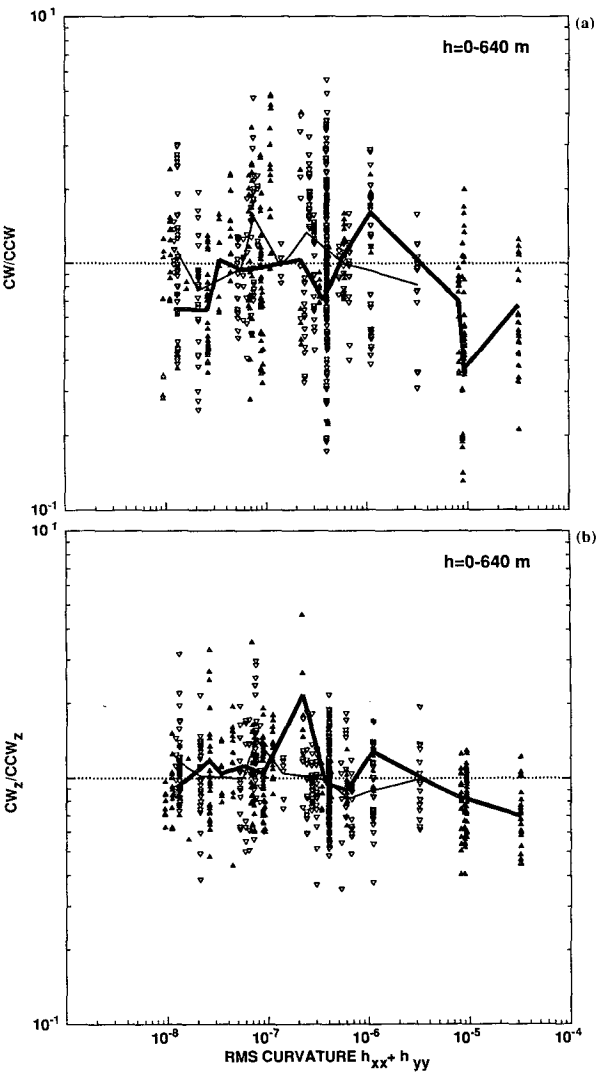

FIG. 8. The ratios of (a) clockwise- to counterclockwise-with-depth energy CW/CCW and (b) clockwise- to counterclockwise-with-depth shear variance CW_z/CCW_z in the bottom 640 m as functions of topographic curvature. Bin averages are shown by solid curves. Open symbols (thin curve) denote concave topography and solid symbols (thick curve) convex topography. Convex topography associated with Caryn Seamount reaches more extreme curvatures than concave topography.

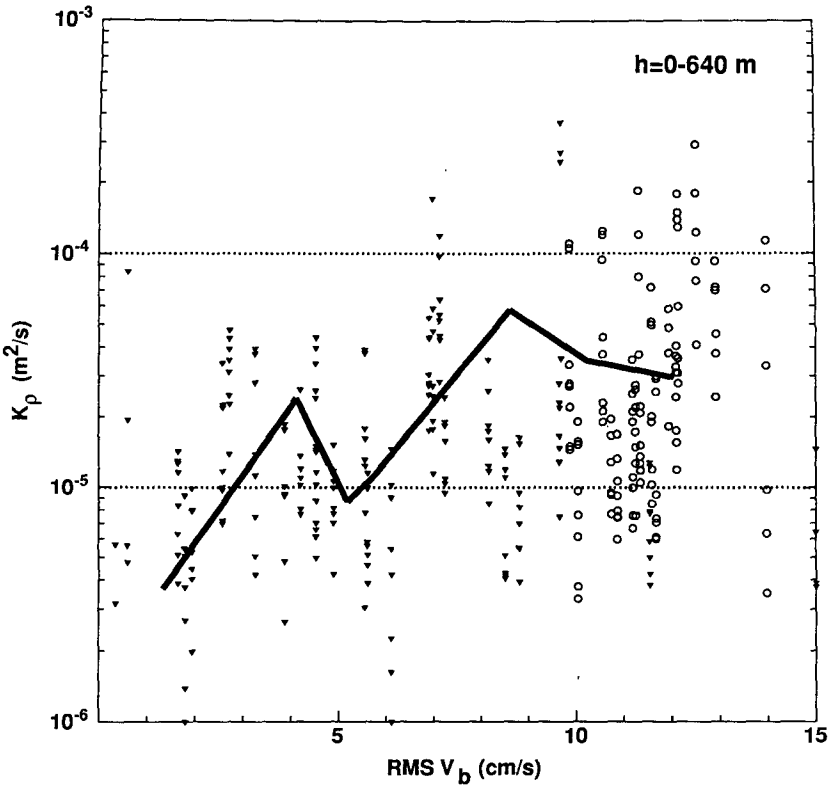

FIG. 9. Inferred eddy diffusivity K_ρ in the bottom 640 m vs near-bottom speeds $|V_b|$ from the POLYMODE profiles. Speeds in excess of 10 cm s^{-1} in the vicinity of the lens profiles (open circles) are due to persistent barotropic southwestward flow in these profiles. Bin averages (solid curve) suggest a tendency for higher abyssal diffusivities to be associated with higher current speeds.

Gilbert and Garrett 1989; Müller and Xu 1992), elevating turbulence production rates. No dependence of eddy diffusivity on rms bottom slope was found here. However, in support of a role for topography, Toole et al. (1994) reports elevated mixing within a few kilometers of an isolated seamount's flanks.

Hydraulic control also produces strong turbulence at sills (Wesson and Gregg 1994) that may dominate average near-bottom mixing. Dramatically elevated eddy diffusivities have recently been found in the abyssal 500 m above sills in the Romanche Fracture Zone ($\sim 100 \times 10^{-4}$ m^2 s^{-1}) and over very rough topography between the Romanche and Chain Fracture Zones ($\sim 10 \times 10^{-4}$ m^2 s^{-1}) in the equatorial Atlantic (Polzin et al. 1996b). Here the turbulence appears to be generated by hydraulically driven flow. Such high diffusivities need only occupy stratified waters over 3% of the ocean bottom to account for all the mixing needed for global budgets. Identifying sites of elevated abyssal mixing and quantifying their intensity are important steps toward understanding the abyssal ocean circulation and global ocean climatology. The consequences of highly localized mixing on the abyssal circulation need to be explored.

Acknowledgments. We thank John Dunlap for his efforts in recovering and maintaining the MODE and POLYMODE data, and Kurt Polzin's guidance on application of the Gregg–Henyey–Polzin parameterization. Collection of the MODE profiles was supported by the Office of Naval Research under Contract N00014-66-C0241 NR 083-004. Collection of the POLYMODE data was funded by the National Science Foundation with Grant OCE 76-24605. Data analysis was supported by National Science Foundation Grant OCE 92-40493 and Office of Naval Research Contract N00014-94-I-0038.

REFERENCES

Armi, L., 1978: Some evidence of boundary mixing in the deep ocean. *J. Geophys. Res.*, **83,** 1971–1979.

Bell, T. H., Jr., 1975: Topographically generated internal waves in the open ocean. *J. Geophys. Res.*, **80,** 320–327.

Cairns, J. L., and G. O. Williams, 1976: Internal wave observations from a midwater float, 2. *J. Geophys. Res.*, **81,** 1943–1950.

Carmack, E. C., and T. D. Foster, 1975: On the flow of water out of the Weddell Sea. *Deep-Sea Res.*, **22,** 711–724.

Duda, T. F., and C. S. Cox, 1989: Vertical wavenumber spectra of velocity and shear at small internal wave scales. *J. Geophys. Res.*, **94,** 939–950.

Elliott, B. A., and T. B. Sanford, 1986a: The subthermohaline lens D1. Part I: Description of water properties and velocity profiles. *J. Phys. Oceanogr.,* **16,** 532–548.
——, and ——, 1986b: The subthermohaline lens D1. Part II: Kinematics and dynamics. *J. Phys. Oceanogr.,* **16,** 549–561.
Eriksen, C. C., 1982: Observations of internal wave reflection off sloping bottoms. *J. Geophys. Res.,* **87,** 525–538.
——, 1996: Internal wave reflection and mixing and Fieberling Guyot. *J. Geophys. Res.,* in press.
Ffield, A., and A. L. Gordon, 1992: Vertical mixing in the Indonesian thermocline. *J. Phys. Oceanogr.,* **22,** 184–195.
Fu, L.-L., 1981: Observations and models of inertial waves in the deep ocean. *Rev. Geophys. Space Phys.,* **19,** 141–170.
Gargett, A. E., 1984: Vertical eddy diffusivity in the ocean interior. *J. Mar. Res.,* **42,** 359–393.
——, 1990: Do we really know how to scale the turbulent kinetic energy dissipation rate ϵ due to breaking of oceanic internal waves? *J. Geophys. Res.,* **95,** 15 971–15 974.
——, P. J. Hendricks, T. B. Sanford, T. R. Osborn, and A. J. Williams III, 1981: A composite spectrum of vertical shear in the upper ocean. *J. Phys. Oceanogr.,* **11,** 1258–1271.
Garrett, C. J. R., and W. H. Munk, 1975: Space–time scales of internal waves: A progress report. *J. Geophys. Res.,* **80,** 291–297.
——, and D. Gilbert, 1988: Estimates of vertical mixing by internal waves reflected off a sloping bottom. *Small-Scale Turbulence and Mixing in the Ocean,* J. C. J. Nihoul and B. M. Jamart, Eds., Elsevier, 405–423.
Gilbert, D., and C. Garrett, 1989: Implications for ocean mixing of internal wave scattering off irregular topography. *J. Phys. Oceanogr.,* **19,** 1716–1729.
Gill, A. E., 1973: Circulation and bottom-water production in the Weddell Sea. *Deep-Sea Res.,* **20,** 111–140.
Gregg, M. C., 1987: Diapycnal mixing in the thermocline: A review. *J. Geophys. Res.,* **92,** 5249–5286.
——, 1989: Scaling turbulent dissipation in the thermocline. *J. Geophys. Res.,* **94,** 9686–9698.
——, and E. Kunze, 1991: Shear and strain in Santa Monica basin. *J. Geophys. Res.,* **96,** 16 709–16 719.
——, D. P. Winkel, and T. B. Sanford, 1993: Varieties of fully-resolved spectra of vertical shear. *J. Phys. Oceanogr.,* **23,** 124–141.
Hautala, S. L., and S. C. Riser, 1989: A simple model of abyssal circulation, including effects of wind, buoyancy and topography. *J. Phys. Oceanogr.,* **19,** 596–611.
Henyey, F. S., 1991: Scaling of internal wave model predictions for ϵ. *Dynamics of Oceanic Internal Gravity Waves, 'Aha Huliko'a Hawaiian Winter Workshop,* P. Müller and D. Henderson, Eds., University of Hawaii at Manoa, 233–236.
——, J. Wright, and S. M. Flatte, 1986: Energy and action flow through the internal wave field. *J. Geophys. Res.,* **91,** 8487–8495.
Hogg, N., P. Biscaye, W. Gardner, and W. J. Schmitz Jr., 1982: On the transport and modification of Antarctic Bottom Water in the Vema Channel. *J. Mar. Res.,* **40**(Suppl.), 231–263.
Huang, R. X., 1989: Simulating the main thermocline in the North Atlantic with an ideal-fluid model. *J. Phys. Oceanogr.,* **19,** 543–547.
Itsweire, E. C., K. N. Helland, and C. W. van Atta, 1986: The evolution of grid-generated turbulence in a stably stratified fluid. *J. Fluid Mech.,* **162,** 299–338.
Jenkins, W. J., 1980: Tritium and ^{3}He in the Sargasso Sea. *J. Mar. Res.,* **38,** 533–569.
Johnson, C. L., and T. B. Sanford, 1980: Anomalous behavior of internal gravity waves near Bermuda. *J. Phys. Oceanogr.,* **10,** 2021–2034.
Kawase, M., 1987: Establishment of deep ocean circulation driven by deep-water production. *J. Phys. Oceanogr.,* **17,** 2294–2317.
Kunze, E., and T. B. Sanford, 1986: Near-inertial wave interactions with mean flow and bottom topography near Caryn Seamount. *J. Phys. Oceanogr.,* **16,** 109–120.
——, M. A. Kennelly, and T. B. Sanford, 1992: The depth dependence of shear finestructure off Point Arena and near Pioneer Seamount. *J. Phys. Oceanogr.,* **22,** 29–41.
Leaman, K. D., 1976: Observations on the vertical polarization and energy flux of near-inertial waves. *J. Phys. Oceanogr.,* **6,** 894–908.
Ledwell, J. R., A. J. Watson, and C. S. Law, 1993: Evidence of slow mixing across the pycnocline from an open-ocean tracer-release experiment. *Nature,* **364,** 701–703.
Lueck, R. G., W. R. Crawford, and T. R. Osborn, 1983: Turbulent dissipation over the continental slope off Vancouver Island. *J. Phys. Oceanogr.,* **13,** 1809–1818.
Luyten, J. E., and H. Stommel, 1991: Comparison of M_2 tidal currents observed by some deep moored current meters with those of the Schwiderski and Laplace models. *Deep-Sea Res.,* **38**(Suppl.), S573–S589.
——, J. Pedlosky, and H. Stommel, 1983: The ventilated thermocline. *J. Phys. Oceanogr.,* **13,** 292–309.
McComas, C. H., and P. Müller, 1981: The dynamic balance of internal waves. *J. Phys. Oceanogr.,* **11,** 970–986.
McEwan, A. D., 1980: Mass and momentum diffusion in internal-wave breaking events. *Stratified Flows 1980 Proc.* Vol. II. J. Carstens and T. McClimans, Eds., Tapir, 742–749.
McWilliams, J. C., 1983: On the mean dynamical balances of the Gulf Stream recirculation zone. *J. Mar. Res.,* **41,** 427–460.
——, and Coauthors, 1983: The local dynamics of eddies in the western North Atlantic. *Eddies in Marine Science,* A. R. Robinson, Ed., Springer-Verlag, 92–113.
The MODE Group, 1978: The Mid-Ocean Dynamics Experiment. *Deep-Sea Res.,* **25,** 859–910.
Morozov, E. G., 1995: Semidiurnal internal wave global field. *Deep-Sea Res.,* **42,** 135–148.
Moum, J. N., and T. R. Osborn, 1986: Mixing in the main thermocline. *J. Phys. Oceanogr.,* **16,** 1250–1259.
——, D. R. Caldwell, and C. A. Paulson, 1989: Mixing in the equatorial surface layer and thermocline. *J. Geophys. Res.,* **94,** 2005–2021.
Müller, P., and N. Xu, 1992: Scattering of oceanic internal gravity waves off random bottom topography. *J. Phys. Oceanogr.,* **22,** 474–488.
Munk, W., 1966: Abyssal recipes. *Deep-Sea Res.,* **13,** 707–730.
——, 1981: Internal wave and smallscale processes. *Evolution of Physical Oceanography,* B. A. Warren and C. Wunsch, Eds., MIT Press, 264–291.
Nabatov, V. N., and R. V. Ozmidov, 1988: Study of turbulence above seamounts in the Atlantic Ocean. *Oceanology,* **28,** 161–166.
Oakey, N. S., 1982: Determination of the rate of dissipation of turbulent energy from simultaneous temperature and velocity shear microstructure measurements. *J. Phys. Oceanogr.,* **12,** 256–271.
Osborn, T. R., 1980: Estimates of the local rate of vertical diffusion from dissipation measurements. *J. Phys. Oceanogr.,* **10,** 83–89.
Padman, L., and T. Dillon, 1991: Turbulent mixing near the Yermak Plateau during CEAREX. *J. Geophys. Res.,* **96,** 4769–4782.
Peters, H., M. C. Gregg, and J. M. Toole, 1988: On the parameterization of equatorial turbulence. *J. Geophys. Res.,* **93,** 1199–1218.
——, ——, and T. B. Sanford, 1995: On the parameterization of equatorial turbulence: Effect of finescale variations below the range of the diurnal cycle. *J. Geophys. Res.,* **100,** 18 333–18 348.
Polzin, K., J. M. Toole, and R. W. Schmitt, 1995: Finescale parameterizations of turbulent dissipation. *J. Phys. Oceanogr.,* **25,** 306–328.
——, N. S. Oakey, J. M. Toole, and R. W. Schmitt, 1996a: Fine- and microstructure characteristics across the northwest Atlantic subtropical front. *J. Geophys. Res.,* in press.
——, K. Speer, J. Toole, and R. Schmitt, 1996b: Intense mixing of Antarctic bottom water in the equatorial Atlantic. *Nature,* **380,** 54–57.
Sanford, T. B., 1991: Spatial structure of thermocline and abyssal internal waves. *Dynamics of Oceanic Internal Gravity Waves, 'Aha Huliko'a Hawaiian Winter Workshop,* P. Müller and D. Henderson, Eds., University of Hawaii at Manoa, 109–142.

——, R. G. Drever, and J. H. Dunlap, 1978: A velocity profiler based on the principles of geomagnetic induction. *Deep-Sea Res.,* **25,** 183–210.

——, ——, and ——, 1985: An acoustic Doppler and electromagnetic velocity profiler. *J. Atmos. Oceanic Technol.,* **2,** 110–124.

Sarmiento, J. L., H. W. Feely, W. S. Moore, A. E. Bainbridge, and W. S. Broecker, 1976: The relationship between vertical eddy diffusion and buoyancy gradient in the deep sea. *Earth Planet. Sci. Lett.,* **32,** 357–370.

Saunders, P. M., 1987: Flow through Discovery Gap. *J. Phys. Oceanogr.,* **17,** 632–643.

Schwiderski, E. W., 1979: Global ocean tides. Part II: The Semidiurnal-Principal Lunar Tide (M_2). *Atlas of Tidal Charts and Maps,* Naval Weapons Center, TR81–142, 87 pp.

Sjöberg, B., and A. Stigebrand, 1992: Computations of the geographical distribution of the energy-flux to mixing processes via internal tides and the associated vertical circulation in the ocean. *Deep-Sea Res.,* **39,** 269–291.

Speer, K. G., and M. S. McCartney, 1992: Bottom water circulation in the western North Atlantic. *J. Phys. Oceanogr.,* **22,** 83–92.

Stommel, H., and A. B. Arons, 1960: On the abyssal circulation of the world ocean—I. Stationary planetary flow patterns on a sphere. *Deep-Sea Res.,* **6,** 140–154.

Sun, H., E. Kunze, and A. J. Williams III, 1996: Vertical heat-flux measurements from a neutrally buoyant float. *J. Phys. Oceanogr.,* **26,** 984–1001.

Thompson, R. O. R. Y., 1980: Efficiency of conversion of kinetic to potential energy by a breaking internal gravity waves. *J. Geophys. Res.,* **85,** 6631–6635.

Toole, J. M., K. L. Polzin, and R. W. Schmitt, 1994: Estimates of diapycnal mixing in the abyssal ocean. *Science,* **264,** 1120–1123.

——, R. W. Schmitt, and K. L. Polzin, 1996: Near-boundary mixing above the flanks of a mid-latitude seamount. *J. Geophys. Res.,* **101,** in press.

Welander, P., 1959: An advective model of the ocean thermocline. *Tellus,* **11,** 309–318.

Wesson, J. C., and M. C. Gregg, 1994: Mixing at Camarinal Sill in the Strait of Gibraltar. *J. Geophys. Res.,* **99,** 9847–9878.

Whitehead, J. A., 1989: Surges of Antarctic Bottom Water into the North Atlantic. *J. Phys. Oceanogr.,* **19,** 853–861.

Wijesekera, H., L. Padman, T. Dillon, M. Levine, C. Paulson, and R. Pinkel, 1993: The application of internal-wave dissipation models to a region of strong mixing. *J. Phys. Oceanogr.,* **23,** 269–286.

Wunsch, C., and S. Webb, 1979: The climatology of deep ocean internal waves. *J. Phys. Oceanogr.,* **9,** 235–243.